

One-Step Synthesis of Antioxidative Graphene-Wrapped Copper Nanoparticles on Flexible Substrates for Electronic and Electrocatalytic Applications

Chi-Ang Tseng,[†] Chiao-Chen Chen,[†] Rajesh Kumar Ulaganathan,[†] Chuan-Pei Lee,[†] Hsu-Cheng Chiang,[†] Chin-Fu Chang,[†] and Yit-Tsong Chen^{*,†,§}

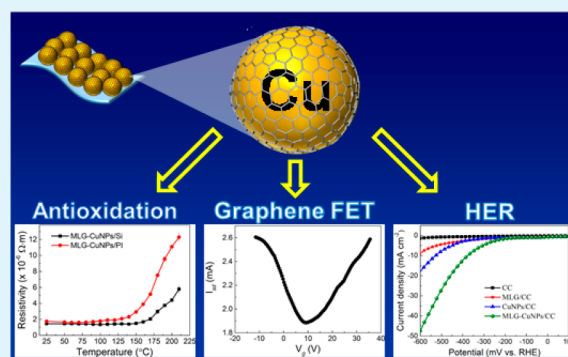
[†]Department of Chemistry, National Taiwan University, No. 1, Sec. 4, Roosevelt Road, Taipei 106, Taiwan

[§]Institute of Atomic and Molecular Sciences, Academia Sinica, P.O. Box 23-166, Taipei 106, Taiwan

Supporting Information

ABSTRACT: In this study, we report a novel, one-step synthesis method to fabricate multilayer graphene (MLG)-wrapped copper nanoparticles (CuNPs) directly on various substrates (e.g., polyimide film (PI), carbon cloth (CC), or Si wafer (Si)). The electrical resistivities of the pristine MLG-CuNPs/PI and MLG-CuNPs/Si were measured 1.7×10^{-6} and 1.4×10^{-6} $\Omega\cdot\text{m}$, respectively, of which both values are ~ 100 -fold lower than earlier reports. The MLG shell could remarkably prevent the Cu nanocore from serious damages after MLG-CuNPs being exposed to various harsh conditions. Both MLG-CuNPs/PI and MLG-CuNPs/Si retained almost their conductivities after ambient annealing at 150 °C. Furthermore, the flexible MLG-CuNPs/PI exhibits excellent mechanical durability after 1000 bending cycles. We also demonstrate that the MLG-CuNPs/PI can be used as promising source-drain electrodes in fabricating flexible graphene-based field-effect transistor (G-FET) devices. Finally, the MLG-CuNPs/CC was shown to possess high performance and durability toward hydrogen evolution reaction (HER).

KEYWORDS: antioxidation, copper nanoparticle, graphene, field-effect transistor, hydrogen evolution reaction



Metal nanoparticles with unique electrical and catalytic properties attracted vast attention in the past decades and have been used for a variety of applications, such as the electrodes for field-effect transistors,¹ organic solar cells,² surface-enhanced Raman scattering,^{3,4} and hydrogen evolution reactions (HER).⁵ In particular, the noble metals, such as gold (Au) and platinum (Pt), have drawn enormous interest due to their high electrical conductivity, excellent oxidation resistivity and prominent electrochemical activity.⁶ However, the high cost of these noble metals has hindered them from practical applications. Therefore, the synthesis of low-cost and earth-abundant metal nanoparticles with superior electrical conductivity and oxidation resistivity has drawn increasing interest in both fundamental research and industrial applications.

Copper nanoparticles (CuNPs) are considered to be a promising candidate to replace most noble metals due to their relatively low cost, nontoxic element and high electrical conductivity. However, when exposing to a room-temperature ambient condition within hours, bare CuNPs are subjected to easy oxidation to form nonconductive copper oxides, which could result in severe degradation in electrical conductivity.⁷ Consequently, how to prevent CuNPs from oxidation to maintain their excellent electrical conductivity is a prerequisite for advanced electronic and electrocatalytic applications.

Graphene, a monolayer of carbon atoms tightly packed into a two-dimensional (2D) honeycomb lattice, has displayed great potential in wide applications,^{8–11} especially for the encapsulation of CuNPs to fabricate flexible electronics because of its exceptional electrical conductivity, impermeability,¹² chemical stability, and high mechanical strength.¹³ For electrode applications, multilayer graphene-encapsulated copper nanoparticles (referred to as MLG-CuNPs) can be designed to protect the enclosed Cu nanocores from oxidation¹⁴ and simultaneously to serve as a conductive contact between individual MLG-CuNPs to maintain electrical transport.¹⁵ Several efforts have recently been reported to synthesize MLG-CuNPs. Lee et al.¹⁶ prepared MLG-CuNPs at 800–900 °C by using solid-phase poly(methyl methacrylate) as a carbon source and found that the solid-phase carbon source can also protect CuNPs from agglomeration during the synthesis. Wang et al.¹⁷ successfully synthesized MLG-CuNPs at 600 °C by using copper(II) acetylacetonate ($\text{Cu}(\text{acac})_2$) as a reaction precursor and proposed a coalescence mechanism for the formation of MLG-CuNPs. First, the gaseous $\text{Cu}(\text{acac})_2$ decomposed at high temperature and created Cu vapor to

Received: May 9, 2017

Accepted: July 20, 2017

Published: July 20, 2017

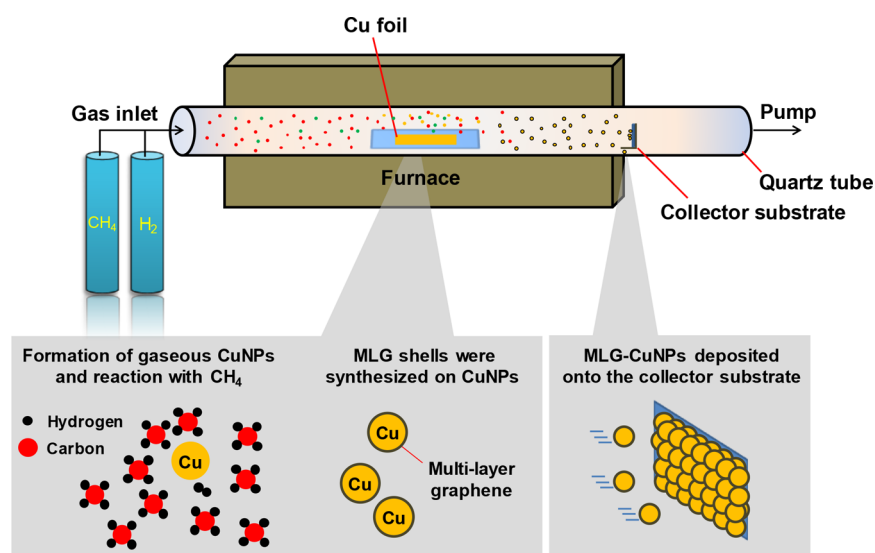


Figure 1. Schematic representation illustrates the experimental setup for the growth of MLG-CuNPs in CVD reaction. A growth mechanism of the as-synthesized MLG-CuNPs is proposed in the lower panels.

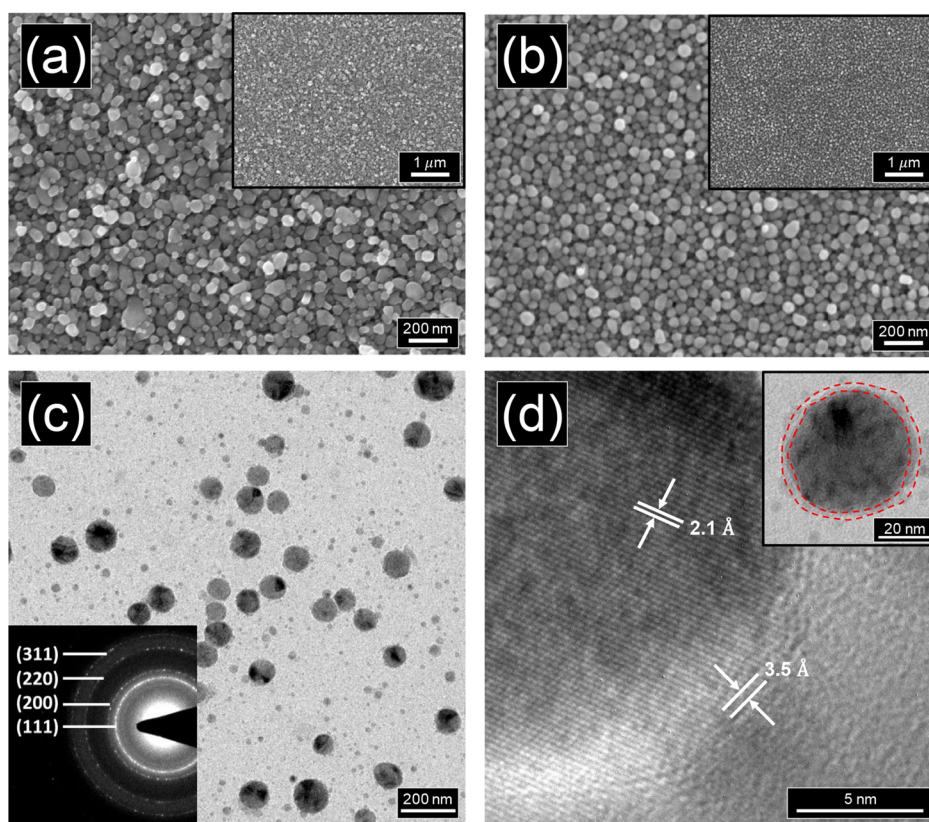


Figure 2. High-magnification SEM images of the as-synthesized (a) MLG-CuNPs/Si and (b) MLG-CuNPs/PI. The insets present the corresponding low-magnification SEM images. (c) TEM image of MLG-CuNPs. The inset displays the SAED pattern of the face-centered cubic (FCC) CuNPs. (d) HR-TEM image of a MLG-CuNP reveals the interlayer spacing (3.5 Å) of graphene and the interplanar distance (2.1 Å) of Cu(111). The inset displays the image of a MLG-CuNP with a ~3 nm-thick MLG shell.

form stable Cu nanoclusters. The Cu nanoclusters acted as a catalyst to facilitate the further decomposition of acetylacetonate radicals and the subsequent adsorption of carbon atoms on the surface of Cu nanoclusters. Because of their high surface activity, the carbon/Cu nanoclusters yielded carbon/Cu nanoagglomerates via collisions. Finally, while the Cu atoms within the carbon/Cu nanoagglomerates coalesced into Cu

nanocores, the carbon atoms diffused out from the nanoagglomerates to develop the MLG. These formation processes were based on the fact that both Cu and carbon atoms have fast interdiffusion rates at a high-temperature CVD reaction and, more importantly, the solubility of carbon in Cu is very low. Although the reports have demonstrated that MLG-CuNPs possess outstanding oxidation resistivity, the harsh synthetic

temperature of the as-synthesized MLG-CuNPs have restricted them from the applications in flexible electronic devices for the next-generation portable display industry. Luechinger et al.¹⁵ prepared a powder of MLG-CuNPs by reducing flame synthesis, where the water-based copper nanocolloids were successfully printed onto a polymer substrate to form a pattern electrode with low electrical conductivity of $\sim 1.5 \text{ S cm}^{-1}$. However, the above-mentioned polymer/carbon encapsulated CuNP electrodes were generally fabricated through a multistep process, such as synthesizing target materials, inkjet printing to form the films on substrates, and sintering to minimize the resistivity of electrodes. Consequently, how to develop a facile one-step method of preparing the antioxidation electrodes of MLG-CuNPs on flexible substrates is highly demanded.

Herein, we report an expeditious chemical vapor deposition (CVD) method (Figure 1 and Section S1 of the Supporting Information) to synthesize MLG-CuNPs by wrapping MLG shells over the Cu nanocores on various substrates (e.g., polyimide film (PI), carbon cloth (CC), or Si wafer (Si)). The advantages of the presented CVD method are thoroughly discussed in Section S1.1 of the Supporting Information. Though the vaporized CuNPs could simultaneously act as a catalyst to facilitate the growth of MLG shells on CuNPs in the high-temperature CVD reaction, the as-grown gaseous MLG-CuNPs flew downstream along the CVD tube to finally deposit on substrates in a low-temperature ($\sim 230 \text{ }^\circ\text{C}$) region. The as-synthesized MLG-CuNPs are highly resistant to oxidation after being exposed to a harsh ambient annealing at $150 \text{ }^\circ\text{C}$ for 3 h and exhibited an excellent mechanical durability through a bending test. For device applications, we demonstrated that MLG-CuNPs/PI can be used as the source-drain electrodes for a flexible graphene-based field-effect transistor (G-FET) device (Section S3 of the Supporting Information). In addition, we found that MLG-CuNPs/CC shows high electrocatalytic activity toward HER in water splitting. More importantly, this MLG-CuNPs/CC electrode possesses an exceptional durability against a harsh alkaline aqueous environment during a long-term electrolysis test.

Figure 2a,b shows the SEM images of closely packed MLG-CuNPs on the Si and PI substrates, respectively, where the size of quasi-circular MLG-CuNPs was calculated to be $52 \pm 9 \text{ nm}$ (Figure S3) from the TEM image (like Figure 2c). The elemental compositions of the MLG-CuNPs were examined by EDX (Figure S4). The crystal structure of CuNPs was analyzed by selected area electron diffraction (SAED, the inset of Figure 2c) to be face-centered cubic (FCC) with four fringes, corresponding to the (111), (200), (220), and (311) crystal planes; notably, no fringes of copper oxides were observed. For further structural characterization, a $\sim 3 \text{ nm}$ -thick MLG shell surrounding the Cu nanocore was observed from the HR-TEM image of a MLG-CuNP (Figure 2d), where the lattice spacings of 2.1 and 3.5 Å consist well with the interplanar separations of Cu(111) and MLG, respectively.¹⁸

Raman scattering spectroscopy was employed to investigate the MLG shells on CuNPs as shown in Figure 3a, containing three well-recognized D, G, and 2D bands at 1360, 1590, and 2690 cm^{-1} , respectively. The D band reflects the disordered sp^2 carbon in graphene, the G band is due to the in-plane C–C stretching,¹⁹ and the 2D peak is caused by the double-resonant Raman scattering by two-phonon emission. The intensity ratios of the 2D to G bands (I_{2D}/I_G) and the D to G bands (I_D/I_G) were measured to be ~ 0.35 and ~ 2.04 , respectively, suggesting that the MLG shell is multilayer and possesses finite crystal

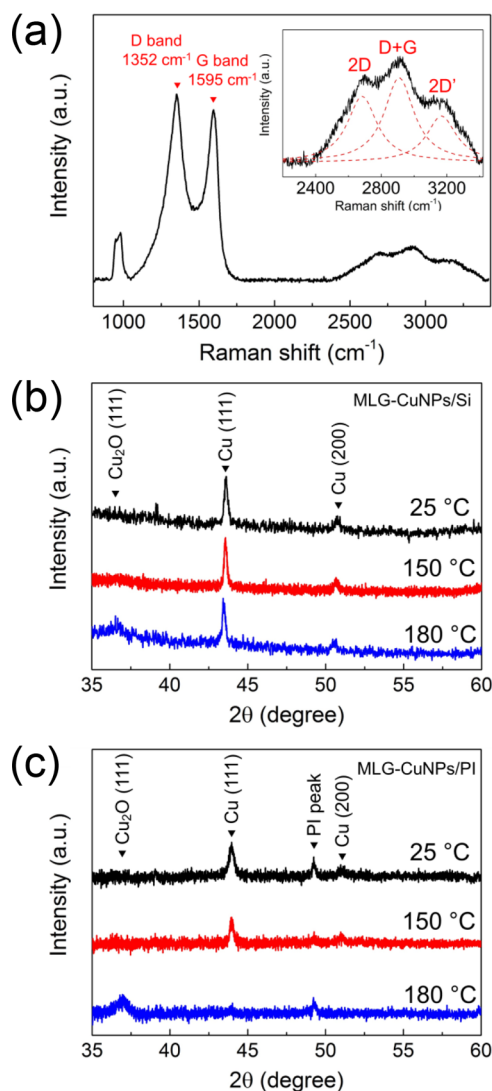


Figure 3. (a) Raman spectrum of the MLG shell after removing the Cu nanocores from MLG-CuNPs. The inset shows the deconvoluted components of the 2D, D + G, and 2D' bands. The XRD spectra of (b) MGL-CuNPs/Si and (c) MGL-CuNPs/PI in a pristine condition ($25 \text{ }^\circ\text{C}$) and after an ambient annealing for 3 h at 150 and $180 \text{ }^\circ\text{C}$, respectively.

sizes and/or plentiful edges of graphene layers. The broad bands at $2400\text{--}3400 \text{ cm}^{-1}$, deconvoluted in the inset of Figure 3a, comprise the 2D (2683 cm^{-1}), D + G (2909 cm^{-1}), and 2D' (3166 cm^{-1}) bands, wherein a nonplanar graphitic structure caused by the strain-induced effect is responsible for the D + G and 2D' bands.¹⁷ Note that this defective structure also benefits the electrocatalytic activity²⁰ toward HER, as will be discussed later.

The thermal stabilities of MLG-CuNPs/Si and MLG-CuNPs/PI were tested by ambient annealing at $\leq 180 \text{ }^\circ\text{C}$ for 3 h. Figure 3b,c shows the XRD spectra of both samples in the pristine condition (at $25 \text{ }^\circ\text{C}$) and after annealing at 150 and $180 \text{ }^\circ\text{C}$. The XRD peaks observed at $2\theta = 43.7^\circ$ and 50.6° are attributed to Cu(111) and Cu(200), respectively. It is interesting that no XRD peaks of copper oxides at $2\theta \sim 35^\circ\text{--}37^\circ$ were observed after ambient annealing of MLG-CuNPs at $150 \text{ }^\circ\text{C}$ for 3 h, suggesting that the Cu nanocore was protected efficiently by the MLG shell from oxidation. However, when MLG-CuNPs were annealed at $180 \text{ }^\circ\text{C}$ for 3

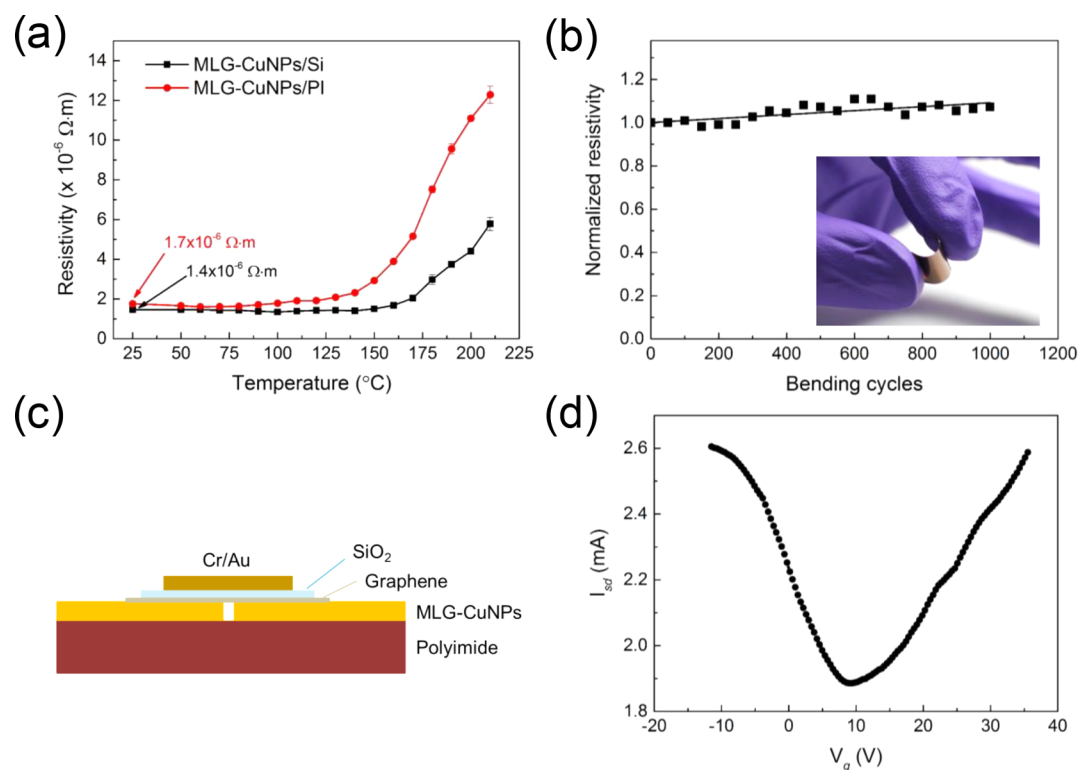


Figure 4. (a) *In situ* temperature-dependent measurements of MLG-CuNPs/Si (black curve) and MLG-CuNPs/PI (red curve) were conducted with a four-probe contact. Every presented data point was collected from the average of six measurements, where the standard deviation of the measured resistivity is less than 5% in the whole temperature range of 50–220 $^{\circ}\text{C}$. (b) Test of the mechanical durability of the MLG-CuNPs/PI electrode was conducted by measuring the electrical resistivity after bending the electrode with a radius of curvature of 1.7 mm for 1000 cycles. The inset shows the digital image of a bendable MLG-CuNPs/PI electrode. (c) Schematic illustration of a G-FET, where MLG-CuNPs are used to fabricate the source-drain electrodes. (d) Transfer curve of the as-fabricated G-FET was obtained from the source-drain current (I_{sd}) vs gate voltage (V_g) measurement at room temperature with a bias voltage of 100 mV.

h, the Cu nanocore oxidized and a weak peak of $\text{Cu}_2\text{O}(111)$ at $2\theta = 36.6^{\circ}$ appeared. Copper oxides could grow at the grain boundaries of the MLG because of the existence of structural defects on the highly curved MLG shell. These XRD investigations indicate that both MLG-CuNPs/Si and MLG-CuNPs/PI sustain their antioxidation abilities in the 3 h annealing up to 150 $^{\circ}\text{C}$. The higher crystallinity of MLG-CuNPs/Si than those of MLG-CuNPs/PI is observed due to the smoother surface of the Si substrate²¹ than that of a PI film (as shown in Figure S5). The complementary XPS measurements and other structural characterizations are also discussed in Section S2.

The *in situ* temperature-dependent resistivity measurements of MLG-CuNPs/Si and MLG-CuNPs/PI at 50–220 $^{\circ}\text{C}$ are displayed in Figure 4a, in which the resistivities of 1.4×10^{-6} and $1.7 \times 10^{-6} \Omega\cdot\text{m}$ for both pristine samples are ~ 100 -fold lower than those of earlier reports.¹⁵ The resistivity of MLG-CuNPs/Si does not alter significantly in the annealing up to 150 $^{\circ}\text{C}$, despite a slight resistivity increase in MLG-CuNPs/PI at 150 $^{\circ}\text{C}$. These results consist with the aforementioned XRD analysis that the Cu nanocore was protected efficiently by the MLG shell from oxidation at ≤ 150 $^{\circ}\text{C}$. The excellent mechanical durability of a flexible MLG-CuNPs/PI was verified by $\sim 7\%$ only increase in resistivity for 1000 bending cycles (Figure 4b). In addition, a flexible G-FET device was fabricated on a PI substrate with a pair of MLG-CuNPs-based source-drain electrodes as illustrated schematically in Figure 4c. The electrical transport of the ambipolar G-FET was characterized by measuring the transfer curve (Figure 4d), where the

obtained mobilities of holes ($\sim 940 \text{ cm}^2 \text{ V}^{-1} \text{ s}^{-1}$) and electrons ($\sim 800 \text{ cm}^2 \text{ V}^{-1} \text{ s}^{-1}$) with a charge neutrality point at ~ 9 V exhibit the active charge carriers of opposite polarities in the unintentionally *p*-doped graphene channel of the as-fabricated G-FET device.

Finally, it is well-known that the use of Cu-based electrodes for the energy research on water splitting was seriously limited due to the poor stability of the Cu-based electrodes in aqueous solution,²² despite the fact that Cu is a highly conductive, earth-abundant, low-cost, and low-toxic catalyst. Nevertheless, with the protection by the MLG shell, MLG-CuNPs may survive in electrochemical reactions. To this end, we synthesized MLG-CuNPs on a flexible carbon cloth substrate (MLG-CuNPs/CC) as an electrocatalytic electrode for HER. The details of electrochemical measurements are shown in Section S4 of the Supporting Information. The application of MLG-CuNPs/CC for HER has several advantages. First, the electrically conductive and chemically stable CC substrate can provide a high surface area for loading MLG-CuNPs. Second, the nanosized CuNPs can further increase the electrocatalytic surface area and electrical conductivity. Third, while the MLG shell can serve as a protective layer with good conductivity, the structural defects on the highly curved MLG shell can beneficially act as an efficient electro-catalyst toward HER in water splitting.

Figure 5a shows the measured polarization curves of HER by employing the bare CC, MLG/CC, CuNPs/CC, and MLG-CuNPs/CC electrodes, respectively. The overpotentials required to drive $J_{\text{cathodic}} = 10 \text{ mA cm}^{-2}$ for the MLG/CC,

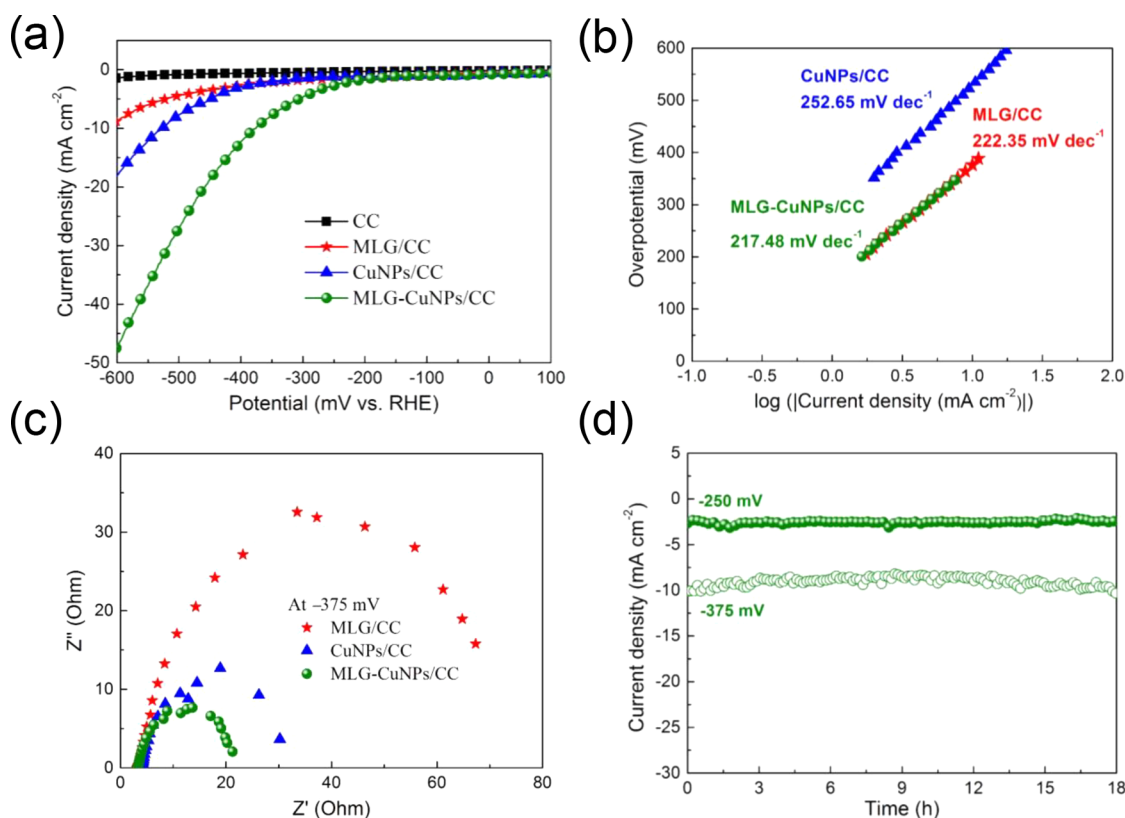


Figure 5. (a) Polarization curves of the bare CC, MLG/CC, CuNPs/CC, and MLG-CuNPs/CC electrodes were measured in N_2 -purged 1 M KOH. All data points are the original results without the iR -correction. (b) Tafel plots of the MLG/CC, CuNPs/CC, and MLG-CuNPs/CC electrodes. (c) Comparison of the Nyquist plots of the MLG/CC, CuNPs/CC, and MLG-CuNPs/CC electrodes, which were measured at an overpotential of -375 mV and scanned from 100 kHz to 10 mHz. (d) Time-dependent cathodic current densities of a MLG-CuNPs/CC electrode were tested for 18 h at the fixed overpotentials of -250 and -375 mV, respectively.

CuNPs/CC, and MLG-CuNPs/CC electrodes are -615 , -530 , and -375 mV, respectively. As compared with several earlier reports,^{23,24} the Cu-based electrocatalytic electrodes usually require the overpotential of at least -400 mV to reach $J_{\text{cathodic}} = 10 \text{ mA cm}^{-2}$. Therefore, the less required overpotential of MLG-CuNPs/CC at -375 mV demonstrates this electrode to be a more active Cu-based electro-catalyst to produce $J_{\text{cathodic}} = 10 \text{ mA cm}^{-2}$. The Tafel plots for the MLG/CC, CuNPs/CC, and MLG-CuNPs/CC electrocatalytic electrodes are displayed in Figure 5b, where the Tafel slopes of all electrodes fall in the short-range of 215–255 mV decade^{-1} , suggesting no dramatic difference in the intrinsic activities of the electrodes.

The Nyquist plot in Figure 5c, obtained from electrochemical impedance spectroscopy (EIS), indicates that MLG-CuNPs/CC has the smallest charge-transfer resistance (R_{ct}) among all of the tested electrodes. A lower R_{ct} value (i.e., with the smaller semicircle) in the Nyquist plot corresponds to the faster charge transfer between electrodes and electrolytes. The smallest R_{ct} of MLG-CuNPs/CC also supports the best HER performance of the MLG-CuNPs/CC electrode in the polarization curve measurements (Figure 5a). It is known that with the lower R_{ct} of MLG-CuNPs/CC, the more efficient charge transport can be achieved, which stems from the synergistic effect on the conductive counterparts between the MLG protective shells and CuNP nanocores. Namely, the MLG shells can remarkably prevent the CuNPs from oxidation (Figures 3b and 3c), thus maintaining the high conductivity of MLG-CuNPs/CC (Figure 4a). In a MLG-CuNP, the CuNP nanocore can act as a scaffold to support the MLG shell, meanwhile preventing the MLG

shell from collapse. In case the hollow MLG shells collapsed to stack to each other (Figure S11), these depressed MLG shells could greatly lose their large charge-transfer surface, resulting in the increase of R_{ct} . By the same token, without the protection of MLG shells, the easily oxidized CuNPs under a harsh environment would retard efficient charge transports, consequently increasing the R_{ct} as well. In contrast, the lower R_{ct} corresponds to the less energy-loss within a system; therefore, a less overpotential is required to drive the HER. As a result, the MLG-CuNPs/CC electrode shows the best HER performance (i.e., the lowest overpotential for achieving $J_{\text{cathodic}} = 10 \text{ mA cm}^{-2}$) and exhibits the lowest R_{ct} value among all electrodes examined. Moreover, a practical application of MLG-CuNPs/CC was also examined by a continuous electrolysis test over 18 h at the fixed potentials of -250 and -375 mV, where the J_{cathodic} values remained stable at ~ 2.5 and $\sim 10 \text{ mA cm}^{-2}$, respectively (Figure 5d). This exceptional durability in the harsh alkaline aqueous environment demonstrates that MLG-CuNPs/CC can be used as a prospective electrode for HER for a long-term operation.

In summary, we have developed a facile one-step CVD method to prepare low-resistance MLG-CuNPs electrodes on a flexible substrate without the requirement of post thermal annealing. The improved electrical resistivities of 1.7×10^{-6} and $1.4 \times 10^{-6} \Omega\cdot\text{m}$ for MLG-CuNPs/PI and MLG-CuNPs/Si are ~ 100 -fold lower than previous reports. The as-synthesized MLG-CuNPs exhibit an excellent antioxidation ability in the annealing up to 150°C . In addition, the flexible MLG-CuNPs/PI possesses an excellent mechanical durability after 1000

bending cycles. A G-FET fabricated on a flexible PI substrate with a pair of MLG-CuNPs-based electrodes shows the hole and electron mobilities of ~ 940 and ~ 800 $\text{cm}^2 \text{V}^{-1} \text{s}^{-1}$, respectively. Finally, the MLG-CuNPs/CC electrode for HER demonstrated a better performance than the electrodes with MLG or CuNPs alone. Besides, this MLG-CuNPs/CC electrode exhibits an exceptional HER durability in alkaline aqueous solution for a long-term period test. We envisage that this novel approach of preparing MLG-CuNPs electrodes on flexible substrates can serve as a simple, cost-effective method to fabricate portable devices in electronic and optoelectronic industries.

■ ASSOCIATED CONTENT

Supporting Information

The Supporting Information is available free of charge on the ACS Publications website at DOI: 10.1021/acsami.7b06490.

CVD synthesis of MLG-CuNPs, material characterizations, MLG-CuNPs-based source-drain electrodes in a G-FET device, and MLG-CuNPs/CC as an electrocatalytic electrode in HER (PDF)

■ AUTHOR INFORMATION

Corresponding Author

*Y.-T. Chen. E-mail: ytcchem@ntu.edu.tw.

ORCID

Yit-Tsong Chen: 0000-0002-6204-8320

Notes

The authors declare no competing financial interest.

■ ACKNOWLEDGMENTS

This work was supported, in part, by the Ministry of Science and Technology (MOST) of Taiwan under Grant Nos. 105-2627-M-002-001 and 103-2113-M-002-014-MY3. We thank the assistance from Ms. Su-Jen Ji for SEM characterizations and from Mr. Hsueh-Ren Chen for TEM operations.

■ REFERENCES

- (1) Jeong, S.; Lee, S. H.; Jo, Y.; Lee, S. S.; Seo, Y.-H.; Ahn, B. W.; Kim, G.; Jang, G.-E.; Park, J.-U.; Ryu, B.-H.; Choi, Y. Air-Stable, Surface-Oxide Free Cu Nanoparticles for Highly Conductive Cu Ink and Their Application to Printed Graphene Transistors. *J. Mater. Chem. C* **2013**, *1*, 2704–2710.
- (2) Tseng, C.-A.; Han, H.-C.; Chong, C.-W.; Chang, C.-C.; Lin, C.-F.; Wang, S.-B.; Tseng, W.-H.; Wu, C.-I.; Lee, J.-H.; Chang, S.-J.; Chen, K.-H.; Chen, L.-C. The Effects of Fluorine-Contained Molecules on Improving the Polymer Solar Cell by Curing the Anomalous S-Shaped I – V Curve. *ACS Appl. Mater. Interfaces* **2015**, *7*, 6683–6689.
- (3) Xu, S.; Man, B.; Jiang, S.; Wang, J.; Wei, J.; Xu, S.; Liu, H.; Gao, S.; Liu, H.; Li, Z.; Li, H.; Qiu, H. Graphene/Cu Nanoparticle Hybrids Fabricated by Chemical Vapor Deposition As Surface-Enhanced Raman Scattering Substrate for Label-Free Detection of Adenosine. *ACS Appl. Mater. Interfaces* **2015**, *7*, 10977–10987.
- (4) Xu, S.; Jiang, S.; Wang, J.; Wei, J.; Yue, W.; Ma, Y. Graphene Isolated Au Nanoparticle Arrays with High Reproducibility for High-Performance Surface-Enhanced Raman Scattering. *Sens. Actuators, B* **2016**, *222*, 1175–1183.
- (5) Berglund, S. P.; He, H.; Chemelewski, W. D.; Celio, H.; Dolocan, A.; Mullins, C. B.P-Si/W2C and P-Si/W2C/Pt Photocathodes for the Hydrogen Evolution Reaction. *J. Am. Chem. Soc.* **2014**, *136*, 1535–1544.
- (6) Sanchez-Romaguera, V.; Wünscher, S.; Turki, B. M.; Abbel, R.; Barbosa, S.; Tate, D. J.; Oyeka, D.; Batchelor, J. C.; Parker, E. a.; Schubert, U. S.; Yeates, S. G. Inkjet Printed Paper Based Frequency Selective Surfaces and Skin Mounted RFID Tags: The Interrelation between Silver Nanoparticle Ink, Paper Substrate and Low Temperature Sintering Technique. *J. Mater. Chem. C* **2015**, *3*, 2132–2140.
- (7) Magdassi, S.; Grouchko, M.; Kamyshny, A. Copper Nanoparticles for Printed Electronics: Routes Towards Achieving Oxidation Stability. *Materials* **2010**, *3*, 4626–4638.
- (8) Xu, S.; Zhan, J.; Man, B.; Jiang, S.; Yue, W.; Gao, S.; Guo, C.; Liu, H.; Li, Z.; Wang, J.; Zhou, Y. Real-Time Reliable Determination of Binding Kinetics of DNA Hybridization Using a Multi-Channel Graphene Biosensor. *Nat. Commun.* **2017**, *8*, 14902.
- (9) Xu, S.; Man, B.; Jiang, S.; Yue, W.; Yang, C.; Liu, M.; Chen, C.; Zhang, C. Direct Growth of Graphene on Quartz Substrates for Label-Free Detection of Adenosine Triphosphate. *Nanotechnology* **2014**, *25*, 165702.
- (10) Liao, C.-D.; Lu, Y.-Y.; Tamalampudi, S. R.; Cheng, H.-C.; Chen, Y.-T. Chemical Vapor Deposition Synthesis and Raman Spectroscopic Characterization of Large-Area Graphene Sheets. *J. Phys. Chem. A* **2013**, *117*, 9454–9461.
- (11) Chen, C. C.; Kuo, C. J.; Liao, C. D.; Chang, C. F.; Tseng, C. A.; Liu, C. R.; Chen, Y. T. Growth of Large-Area Graphene Single Crystals in Confined Reaction Space with Diffusion-Driven Chemical Vapor Deposition. *Chem. Mater.* **2015**, *27*, 6249–6258.
- (12) Schriver, M.; Regan, W.; Gannett, W. J.; Zaniwski, A. M.; Crommie, M. F.; Zettl, A. Graphene as a Long-Term Metal Oxidation Barrier: Worse than Nothing. *ACS Nano* **2013**, *7*, 5763–5768.
- (13) Zhu, J.; Yang, D.; Yin, Z.; Yan, Q.; Zhang, H. Graphene and Graphene-Based Materials for Energy Storage Applications. *Small* **2014**, *10*, 3480–3498.
- (14) Stankovich, S.; Dikin, D. a.; Dommett, G. H. B.; Kohlhaas, K. M.; Zimney, E. J.; Stach, E. a.; Piner, R. D.; Nguyen, S. T.; Ruoff, R. S. Graphene-Based Composite Materials. *Nature* **2006**, *442*, 282–286.
- (15) Luechinger, N. A.; Athanassiou, E. K.; Stark, W. J. Graphene-Stabilized Copper Nanoparticles as an Air-Stable Substitute for Silver and Gold in Low-Cost Ink-Jet Printable Electronics. *Nanotechnology* **2008**, *19*, 445201.
- (16) Lee, S.; Hong, J.; Koo, J. H.; Lee, H.; Lee, S.; Choi, T.; Jung, H.; Koo, B.; Park, J.; Kim, H.; Kim, Y.-W.; Lee, T. Synthesis of Few-Layered Graphene Nanoballs with Copper Cores Using Solid Carbon Source. *ACS Appl. Mater. Interfaces* **2013**, *5*, 2432–2437.
- (17) Wang, S.; Huang, X.; He, Y.; Huang, H.; Wu, Y.; Hou, L.; Liu, X.; Yang, T.; Zou, J.; Huang, B. Synthesis, Growth Mechanism and Thermal Stability of Copper Nanoparticles Encapsulated by Multi-Layer Graphene. *Carbon* **2012**, *50*, 2119–2125.
- (18) Ishigami, M.; Chen, J. H.; Cullen, W. G.; Fuhrer, M. S.; Williams, E. D. Atomic Structure of Graphene on SiO₂. *Nano Lett.* **2007**, *7*, 1643–1648.
- (19) Pimenta, M. a.; Dresselhaus, G.; Dresselhaus, M. S.; Cançado, L. G.; Jorio, A.; Saito, R. Studying Disorder in Graphite-Based Systems by Raman Spectroscopy. *Phys. Chem. Chem. Phys.* **2007**, *9*, 1276–1291.
- (20) Punckt, C.; Pope, M. A.; Liu, J.; Lin, Y.; Aksay, I. A. Electrochemical Performance of Graphene as Effected by Electrode Porosity and Graphene Functionalization. *Electroanalysis* **2010**, *22*, 2834–2841.
- (21) Lee, J.; Kwak, S. H.; Kim, H. J. Effects of Substrates Roughness on c-Axis Preferred Orientation of ZnO Films Deposited by Rf Magnetron Sputtering. *Thin Solid Films* **2003**, *423*, 262–266.
- (22) Paracchino, A.; Mathews, N.; Hisatomi, T.; Stefik, M.; Tilley, S. D.; Grätzel, M. Ultrathin Films on Copper(i) Oxide Water Splitting Photocathodes: A Study on Performance and Stability. *Energy Environ. Sci.* **2012**, *5*, 8673.
- (23) Du, J.; Wang, J.; Ji, L.; Xu, X.; Chen, Z. A Highly Active and Robust Copper-Based Electrocatalyst toward Hydrogen Evolution Reaction with Low Overpotential in Neutral Solution. *ACS Appl. Mater. Interfaces* **2016**, *8*, 30205–30211.
- (24) Kumar, B.; Saha, S.; Basu, M.; Ganguli, A. K. Enhanced Hydrogen/oxygen Evolution and Stability of Nanocrystalline (4–6 nm) Copper Particles. *J. Mater. Chem. A* **2013**, *1*, 4728–4735.